IMPACT OF DIFFERENTIAL TORSIONAL ROTOR CANT ON THE FLIGHT CHARACTERISTICS OF A PASSENGER-GRADE QUADROTOR

Kagan Atci kagan.atci@dlr.de
Tim Jusko tim.jusko@dlr.de
Alexander Štrbac alexander.strbac@dlr.de
Feyyaz Guner feyyaz.guener@dlr.de

Institute of Flight Systems
German Aerospace Center (DLR)
Lilienthalplatz 7, D-38108, Braunschweig, GERMANY

Abstract
At the Institute of Flight Systems at DLR, studies have been performed to understand the flight characteristics of novel eVTOL configurations. As part of these studies, previously conducted handling qualities assessments on a 2-passenger quadrotor configuration had revealed major deficiencies about its yaw axis. Based on this result, the quadrotor model has been modified by differential torsional canting to improve its yaw characteristics. This paper analyzes the resulting impacts of such modification on the flight performance, dynamic stability and handling qualities. A piloted virtual flight test campaign was conducted to assess predicted and assigned handling qualities levels in compliance with the quantitative and qualitative performance standards of ADS-33E. The results show an improvement in midterm yaw response at the expense of increase in total required power. The pilot ratings and comments also confirm the improvement on the yaw response upon the flown MTEs.

NOMENCLATURE

Symbols

χ_d	differential torsional cant angle	°
δ_0, δ_p	collective and pedal inputs	%
δ_x, δ_y	longitudinal and lateral cyclic inputs	%
λ	eigenvalue of the state matrix	rad/s
$L_{..}$, $M_{..}$, $N_{..}$	moment derivatives	
Ω_i	rotational speed of the i-th rotor	rpm
ϕ_i, θ_i	local tilting angles of the i-th rotor	°
ϕ, θ, ψ	roll, pitch, yaw angle	rad
p, q, r	roll, pitch, yaw rates	rad/s
Ψ_i	orientation of the i-th rotor to center	°
u, v, w	body-fixed velocities	m/s
$X_{..}$, $Y_{..}$, $Z_{..}$	force derivatives	
ζ	damping ratio	–

Acronyms

ACAH	Attitude Command/Attitude Hold
ACT/FHS	Active Control Technology / Flying Helicopter Simulator
AVES	Air VEhicle Simulator
BWS	Bedford Workload Scale
CPACS	Common Parametric Aircraft Configuration Schema
eVTOL	Electric Vertical Take-off and Landing
GVE	Good Visual Environment
HOST	Helicopter Overall Simulation Tool
HQR	Cooper-Harper Handling Qualities Rating Scale
MTE	Mission Task Element
RC	Rate Command

1. INTRODUCTION

The interest in eVTOLs has been growing since the last decade. Currently, there are more than 600 registered eVTOLs in the World eVTOL Aircraft Directory of the Vertical Flight Society [1], divided into multiple categories with a broad spectrum of use cases.

Quadrotors are one of the well-established candidates among the eVTOL concepts categorized under multirotor configurations. Quadrotor configurations distribute the thrust between an array of four rotors, usually vectoring parallel to each other. These rotors mostly have an rpm-driven architecture, where each rotor is powered by an electric motor. The use of electric motors enables less complexity and lower mass by eliminating sophisticated parts, such as swashplates, bearings, hinges and transmission.

Quadrotor vehicles are controlled by varying the rotational speed and thereby the thrust in individual rotors using conventional helicopter inceptors. The maneuvers around the lateral and longitudinal axes (roll & pitch) are achieved by the anti-symmetric thrust along these axes, whereas the differential torque of the rotors is employed in order to initiate maneuver around the vertical axis (yaw).

In the previous study [2], the linear flight dynamics and handling qualities of a passenger-grade quadrotor was investigated based on the criteria and mission task elements given in the ADS-33E [3]. The linear flight dynamics analyses revealed unstable phugoid modes about the pitch and roll axes. Furthermore, the criteria-based handling qualities prediction revealed poor yaw characteristics. These undesired flying characteristics were also reflected on the handling qualities ratings of the pilots falling mostly between Level 2 and 3 with respect to the Cooper-Harper Handling Qualities Rating Scale (HQR) [4].

In the current work, a couple of improvements have been applied to the flight model. In that regard, the model has been equipped with a stability augmentation system. However, even the stability augmentation system doesn't provide sufficient improvement in the yaw characteristics, since their origin is the lack of adequate torque difference while initiating the yaw motion. Therefore, a constructive approach is required. In this regard, Niemiec et. al. [5] investigated the effects of multiple flapwise and torsional canting modes on the trim and flight dynamics of a small-scale quadrotor drone. They showed that a differential torsional canting mode can increase the yaw authority of the vehicle by up to 325 %. In addition, the roll sensitivity is further increased, while the pitch sensitivity is reduced due to change in the rotor flow conditions resulting from the rotor cant. To investigate the effects of this approach on a larger scale quadrotor vehicle, the flight model form the previous study [2] has been modified by applying the differential torsional cant.

A detailed definition of rotor canting is given in [5]. According to this definition, the torsional cant (χ) is described as the tilt of the rotor about the axis extending radially from the geometric center of the vehicle towards the rotor hub called the boom axis. As is illustrated in Figure **1**, the rotor plane sets a new orientation along its canted axis. The resulting inclinations of the rotors are shown with red arrows indicating the canting direction with respect to the body-fixed xy-plane. Depending on the canting mode, a positive or negative χ is applied to the individual rotors. As there are four separate torsional canting modes introduced, Figure **1** illustrates an example of the *differential* torsional canting mode, which is the focused model modification in this study.

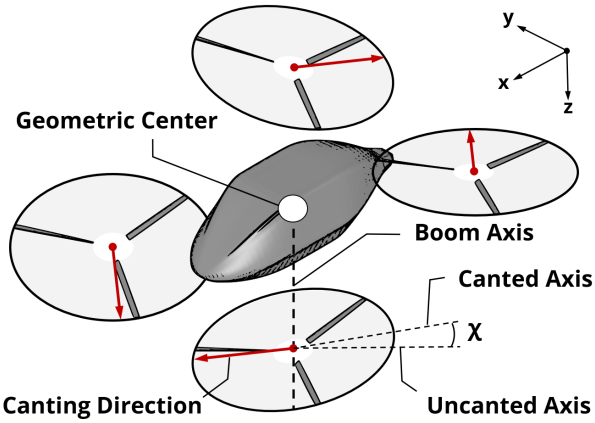

Figure 1 Torsional canting on quadrotor

This study aims to show the impacts of the differential torsional rotor cant on the flight characteristics of a passenger-grade quadrotor in terms of trim performance, flight dynamics, and handling qualities. The paper starts with the technical approach, introducing the process flow, as well as the baseline and the modified variants of the quadrotor model used. This is followed by the trim analysis comparison between the baseline and the modified variants. Thereafter, linear time-invariant models of these variants are compared at hover state. Next, the handling qualities of the baseline variant and one selected modified variant are compared by offline criteria and pilot ratings on the flown MTEs for the hover and low-speed regime in the flight simulator. Finally, conclusions of the study are given.

2. TECHNICAL APPROACH

The technical approach incorporates automated steps in a framework. The models are created using the CPACS [6] data format. The aeromechanical computations take place in HOST [7] provided by Airbus Helicopters. Three main types of computations are available in HOST. These are trim analysis, linear time-invariant modeling and non-linear time domain simulation. The piloted test campaign is conducted in the flight simulator AVES [8], a research simulation facility operated by the Institute of Flight Systems at DLR in Braunschweig.

Figure **2** shows the process flow of the framework. Initially, the model parameters are gathered in a table within Excel. Then, the CPACS file of the vehicle model is created through a Python script (CPACS MODELER) by reading these parameters. The CPACS file contains all the necessary data for the computations. Moreover, the model geometry can be visualized using TIGLViewer [9] developed for CPACS. The HOST model is derived from CPACS file using the in-house developed tool-wrapper CPACS4HOST (C4H). The created model can be used both in offline analysis and real-time simulation. In the case of offline analysis, C4H updates the CPACS file with the result data delivered by HOST. Thus, the whole process from parameterization to final analysis is contained in a single file. As for the piloted simulation, a non-linear real-time simulation can be initiated in AVES with HOST continuously running in the background using the same model files (more details in Section **5**).

Following sections give details of the design and modeling of the baseline and modified quadrotor configurations.

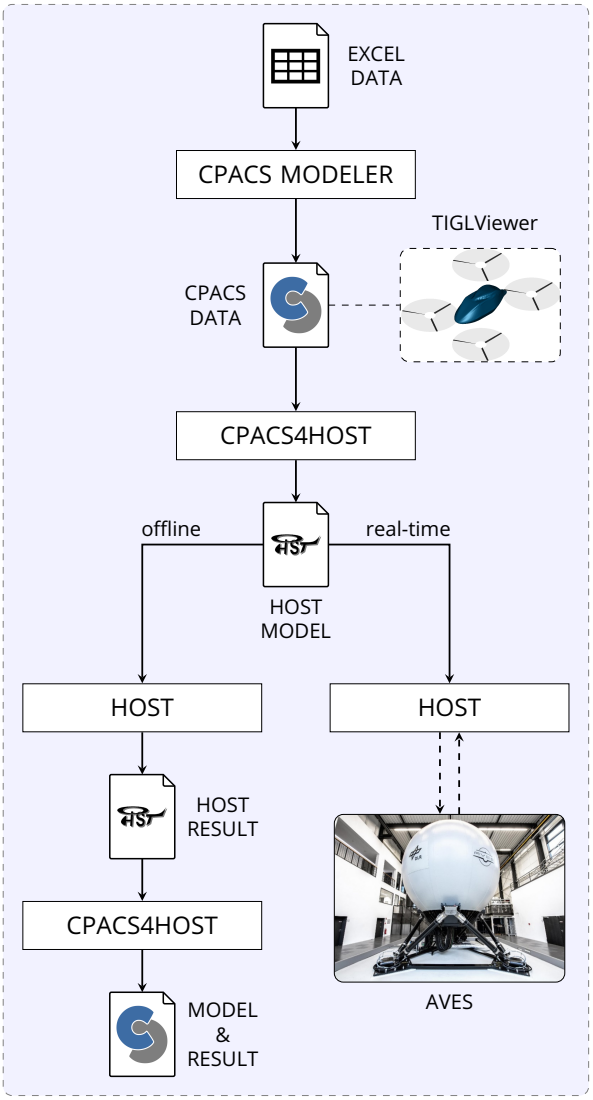

Figure 2 Framework process flow

2.1. Modeling of the Quadrotor

The studied baseline configuration is taken from the parameterized model given in [10], which is a two-passenger rpm-controlled quadrotor configuration sized with respect to the urban air mobility mission requirements of NASA. The mission profile consists of two separate legs with $37.5\,\mathrm{nmi}$ each to be flown at a headwind of $10\,\mathrm{kts}$ with a reserve of 20 minutes [11], [12], [13]. Table **1** shows the parameters of the baseline configuration, while Figure **3** depicts a representative visualization of this model. Parameters that have not been provided are complemented with additional data.

The fuselage aerodynamics are modeled with a simple drag area of $D/q = 0.6\,\mathrm{m}^2$, based on the given data of conceptual quadrotor models with different passenger sizes [11], [14], where D is the cruise drag and q is the dynamic pressure. Here, the assumed drag area contains the wetted area of the fuselage along with the under-carrige, faired rotor hubs and support arms.

The rotors are placed in a cross arrangement equidistantly from the geometric center in lateral and longitudinal direction by the factor $\mathrm{a} = 1.25$, multiplied with the rotor radius. Here, the geometric center is also the location of the center of gravity and the fuselage aerodynamic center. This approach neglects the moments that occur due to the offset positioning of the force elements, hence provides equal thrust distribution onto rotors in hover. Moreover, the forward and aft rotors are separated in vertical direction. Although the rotor-rotor interaction is neglected, study shows that such separation in vertical direction can reduce the power up

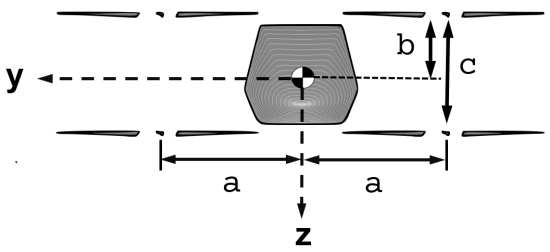

(a) Front view

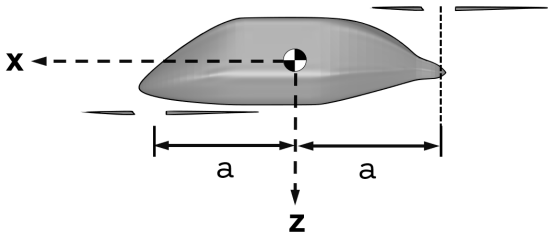

(b) Side view

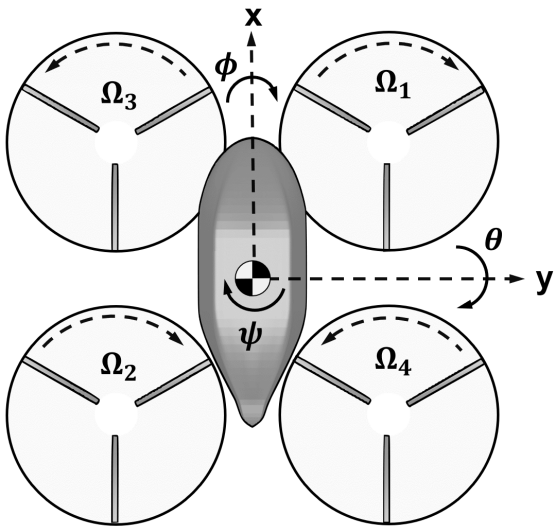

(c) Top view

Figure 3 Visualization of the baseline configuration (*see **Rotor** in Table **1** for* a, b *and* c)

to $4.5\,\%$ in forward flight [11]. First, the aft rotors are vertically positioned with respect to the center of gravity by a distance of b and the forward rotors are positioned by a distance determined by factor c, to be multiplied by the rotor radius. The rotor blades are modeled as rectangular planform using blade element theory. For the aerodynamic profile, the NACA 23012 is chosen, which is a widely popular airfoil in the rotor blade design. The blade is twisted with a constant angle of $35°$ at the root and a linear distribution of $-18.4\,°/\mathrm{m}$, such that the tip profile remains untwisted.

Table 1 Design parameters of the baseline configuration (** *identifies the complemented parameters)*

Parameter	Unit	Value
Cell		
Gross mass	kg	1039
Moment of inertia		
I_{xx} - along x axis	$\mathrm{kg\,m^2}$	2878
I_{yy} - along y axis	$\mathrm{kg\,m^2}$	2878
I_{zz} - along z axis	$\mathrm{kg\,m^2}$	3482
Fuselage		
Drag area (D/q)**	$\mathrm{m^2}$	0.6
Rotor		
Disc loading	$\mathrm{N/m^2}$	143.65
Radius	m	2.38
Rotational speed	rpm	624.6
Blade number	—	3
Mass	kg	13.40
Inertia	$\mathrm{kg\,m^2}$	37.94
Lock number	—	3.65
Rotor positioning** (*see Figure **3***)		
a - Hor. rotor spacing	—	1.25
b - Rear rotor z-pos.	m	0.9
c - Vert. rotor spacing	—	0.9
Blade		
Chord	m	0.137
Root twist**	°	35
Twist slope**	°/m	-18.4

Figure **3c** shows the rotor indexing and rotational directions along with the vehicle orientation in the body-fixed coordinate system. It should be noted that the positive rotor rotational direction for each Ω_i acts in the counter-clockwise (CCW) direction, whereas the positive yaw motion ψ acts in the clockwise (CW) direction. In that respect, rotors 1 and 2 rotate in negative sense, and rotors 3 and 4 rotate in positive sense.

2.2. Differential Torsional Canting

Differential torsional canting is one of the four introduced torsional rotor canting modes by [5]. As schematized in Figure **4**, this mode alternates the torsional canting of the individual rotors in a positive or negative sense in a way that the resulting thrust symmetry in hover is not violated. In addition, the in-plane thrust component of each rotor con-

tributes to yaw acceleration without any lateral or longitudinal acceleration. Unlike in the original definition, CW-rotating rotors are canted negatively and the CCW-rotating rotors are canted positively in the configuration studied. This canting mode is denoted by the canting angle vector

$$\boldsymbol{\chi} = \left(-\chi_d, -\chi_d, \quad \chi_d, \quad \chi_d\right) \tag{1}$$

where the positive angle χ_d is the same for each rotor.

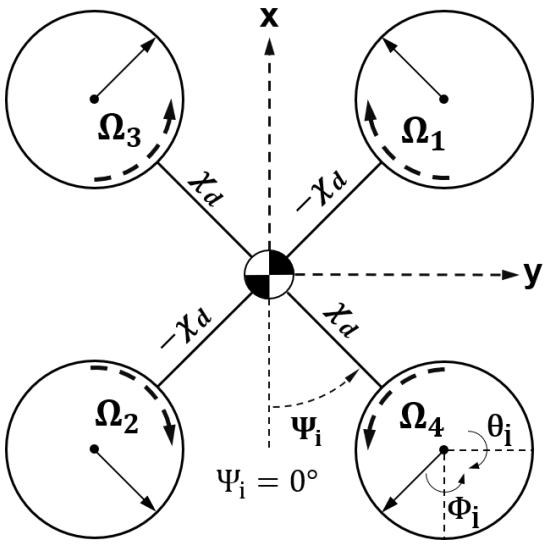

Figure 4 Canted quadrotor configuration schema

Since the rotors are canted relative to the rotor boom axis, a transformation is applied to obtain the rotor orientation relative to the aircraft frame. The orientation of the i-th rotor with respect to the aircraft roll axis (x) is defined by the angle ϕ_i, while the orientation about the pitch axis (y) is defined by θ_i as shown in Figure **4**. Given the rotor azimuth angle (Ψ_i), the orientation of each rotor is calculated by the following relation

$$\begin{aligned} \phi_i &= -\boldsymbol{\chi}_i \cos\Psi_i \\ \theta_i &= \quad \boldsymbol{\chi}_i \sin\Psi_i \end{aligned} \tag{2}$$

for $i = 1, 2, 3, 4$. In this regard, the parameterization of ϕ_i and θ_i with respect to their ψ_i is given in Table **2**.

3. TRIM ANALYSIS

The baseline model ($\chi_d = 0°$) is trimmed from hover state to $150\,\mathrm{km/h}$ forward flight under standard atmospheric conditions. The trim characteristics of the modified models canted by $2.5°$, $5°$ and $7.5°$ are compared with respect to the baseline trim characteristics. The results are shown in Figures **5** to **8**, respectively.

Table 2 Differential torsional canting parameterization of the quadrotor configuration

i	Ψ_i [°]	ϕ_i [°]	θ_i [°]
1	135	$\chi_d\sqrt{2}/2$	$\chi_d\sqrt{2}/2$
2	315	$-\chi_d\sqrt{2}/2$	$-\chi_d\sqrt{2}/2$
3	225	$\chi_d\sqrt{2}/2$	$-\chi_d\sqrt{2}/2$
4	45	$-\chi_d\sqrt{2}/2$	$\chi_d\sqrt{2}/2$

In Figure **5**, the left plot illustrates the thrust of the front and rear rotors specified by the rotor area, the middle plot shows the pitch attitude of the vehicle, and the right plot shows the total power required for the baseline model. At the hover condition, all rotors create identical thrust, corresponding to a disc loading of $143.65\,\mathrm{N/m^2}$ as stated in Table **1**. The forward flight is achieved through pitch-down attitude of the vehicle, where the rotors are vectored towards the flight direction, in order to create horizontal thrust for overcoming the drag. To maintain this attitude, rear rotors produce higher thrust, while front rotors produce less thrust. This tendency can be traced at an increasing rate up to $65\,\mathrm{km/h}$ horizontal speed. From this point on, the tendency starts to decrease, as the front rotors spin faster to compensate the increasing pitch-down moment of the fuselage. The pitch-down attitude increases with a linear rate and reaches $-10°$ at $150\,\mathrm{km/h}$. The total power is put together through induced drag resulting from the air inflow through the rotors, blade profile drag and parasite drag of the fuselage. The maximum total power in low-speed region is located at hover due to the dominance of the induced power. With increasing edgewise flow of the rotor blades in forward flight, the induced power declines, which leads to a drop in the total power. The minimum required power is reached at about $65\,\mathrm{km/h}$, which is the speed, where the rotors partially start to work against fuselage pitch-down moment. Likewise, the increasing parasite drag of the fuselage begins dominating the total power from that point on. Since the blade pitch is not adjustable, vectoring the rotors towards the flight direction also causes higher profile drag that contributes to the increment of the total power in high-speed region. Therefore, it is essential to consider the aspects of the blade design for rpm-controlled rotors separately from pitch-controlled rotors.

Figure **6** shows the specific thrust of the modified variants compared relative to the baseline model.

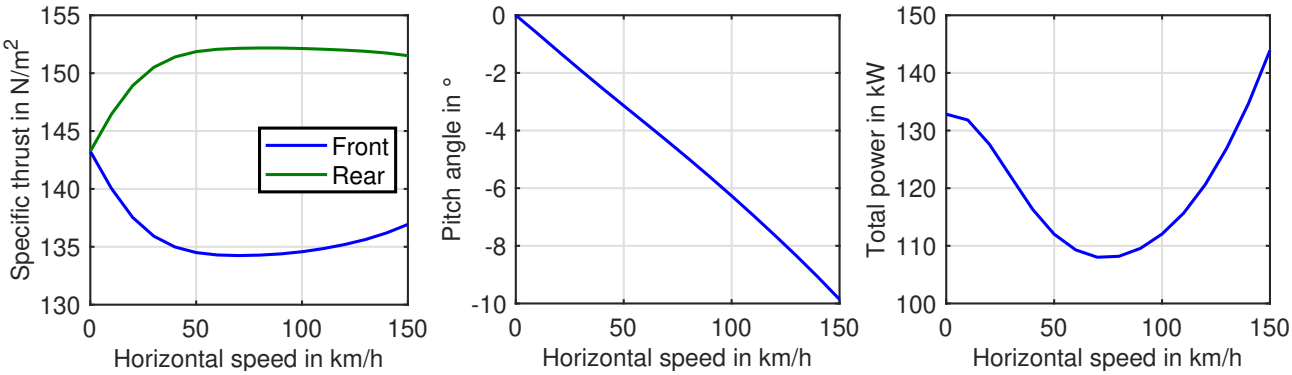

Figure 5 Trim characteristics of the baseline model ($\chi_d = 0°$) in forward flight

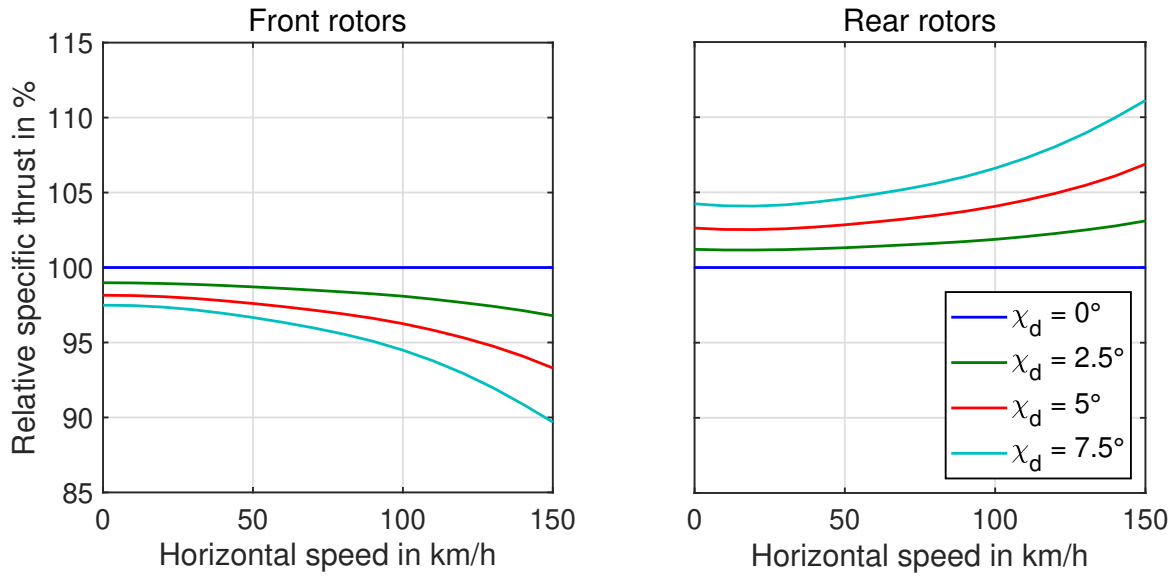

Figure 6 Specific thrust comparison relative to the baseline model

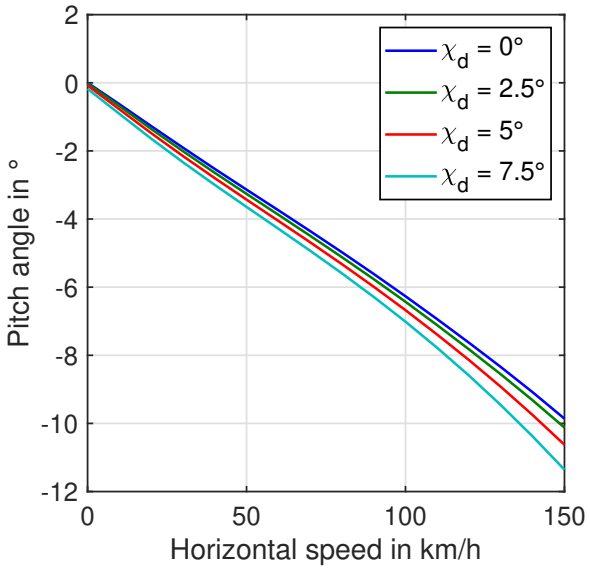

Figure 7 Pitch angles of the baseline and modified models

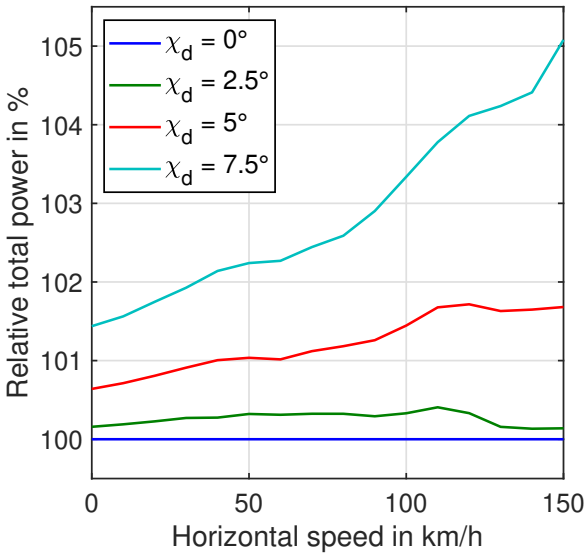

Figure 8 Total required power comparison relative to the baseline model

It can be seen that the specific thrust values of the front and rear rotors separate asymmetrically as the canting angle grows. There are two main constraints causing this separation. To understand the problem, the longitudinal and vertical force components acting on the vehicle at hover are illustrated in Figure **9**. The first constraint is the decrement of the vertical thrust component ($F_{z,front}$ and $F_{z,rear}$) in the rotors. To compensate the loss of thrust in the vertical direction resulting from the canting mode, the rotors should produce higher thrust, which triggers the second constraint. Combined with the vertical rotor separation, torsional differential canted rotors create a nose-up pitching moment M_{χ_d} about the center of gravity resulting from the longitudinal opposite force component of the canted rotors ($F_{x,front}$ and $F_{x,rear}$). To satisfy these two constraints while maintaining the hover trim, rear rotors carry out the bigger portion of the vertical thrust, while front rotors set in a relatively lower thrust in order to cancel out the pitching moment. It has to be noted that the thrust separation between the front and rear rotors isn't distributed evenly. At hover, the rear rotors of the $\chi_d = 2.5°$ variant produce $1.2\,\%$ higher thrust relative to baseline, where front rotors produce $1\,\%$ less from baseline. For $\chi_d = 5°$, this separation is $2.6\,\%$ to $-2\,\%$, and for $\chi_d = 7.5°$, it is $4.2\,\%$ to $-2.5\,\%$. This trend remains apparent throughout the entire speed spectrum while increasing in magnitude for higher speeds.

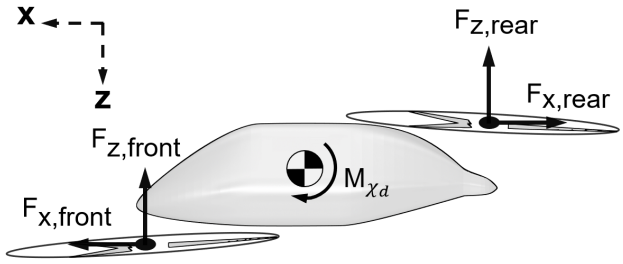

Figure 9 Rotor forces and resulting moment about the center of gravity in hover condition

Figure **7** shows the pitch attitude of all compared models. It can be seen that the canted models can maintain the hover at $\theta = 0°$, since the rear rotors cancel out the pitching moment as mentioned previously. However, the differential torsional cant leads to a slightly more nose-down tendency in forward flight. Since these nose-down attitude deviations are considerably small, a noticeable difference can only be observed at models with higher cant angle, e.g., starting from $\chi_d = 5°$. This can be considered as a small trade-off due to the relaxation of the front rotors in forward flight, so that the faster spinning rear rotors have to be further vectored towards the flight direction in order to compensate the drag.

Figure **8** shows the total required power of the canted models relative to the baseline model. The alteration of the total power for $\chi_d = 2.5°$ variant is negligibly low with a $0.4\,\%$ deviation at its maximum. The $\chi_d = 5°$ variant has a maximum deviation of $1.7\,\%$, while this value lies at $5.1\,\%$ for $\chi_d = 7.5°$. At hover as well as in the low-speed regions, the offset between the curves occurs mainly due to the overall increment at the induced drag and profile drag. As these parameters highly correlate with the generated thrust, the induced power and profile power of the canted rear rotors increase by a greater amount than those of the front rotors that decrease, causing a total power increment. With the horizontal speed increasing, the profile drag in the rear rotors becomes more dominant, as the flow conditions get inefficient due to the shallower disc angle resulting from partially back tilted rotors. These inefficient conditions cause the growth of stall areas emerging in the rotor disc at high speeds, degrading the generated thrust. To overcome this thrust degradation, rear rotors spin even faster, leading to a higher increment in the profile drag. This shows the need of a special blade design for the rear rotors, if the rotors are subjected to differential torsional rotor canting. Apart from induced and profile power, the parasite power doesn't significantly contribute to the change in the total power, since the pitch attitudes of all variants are close.

4. LINEAR FLIGHT DYNAMICS

A linear quadrotor flight model is needed to assess the influence of differential torsional canting on the flight dynamics in terms of stability derivatives. Therefore, non-linear models of the baseline ($\chi_d = 0°$) and modified variants ($\chi_d = 2.5°$, $5°$ and $7.5°$) are numerically linearized around the hover trim condition. It is worth mentioning that the vehicle axes are completely decoupled in quadrotor configurations, unlike in the standard helicopter configurations with main rotor-tail rotor arrangement. Hence, the dynamic properties of each axis can be studied separately.

The linearized bare-airframe model structure is given in state-space form by

$$\dot{\mathbf{x}} = \mathbf{A}\mathbf{x} + \mathbf{B}\mathbf{u} \tag{3}$$

with the state and control vectors given as

$$\begin{aligned} \mathbf{x} &= \begin{bmatrix} u & v & w & p & q & r & \phi & \theta & \psi \end{bmatrix}^T \\ \mathbf{u} &= \begin{bmatrix} \delta_0 & \delta_x & \delta_y & \delta_p \end{bmatrix}^T \end{aligned} \tag{4}$$

The system matrix **A** and the control matrix **B** are obtained following the numerical linearization. For the initial trim state at hover conditions, the **A** and **B** matrices are

$$\mathbf{A} = \begin{bmatrix} X_u & 0 & 0 & 0 & X_q & 0 & 0 & -g & 0 \\ 0 & Y_v & 0 & Y_p & 0 & 0 & g & 0 & 0 \\ 0 & 0 & Z_w & 0 & 0 & 0 & 0 & 0 & 0 \\ 0 & L_v & 0 & L_p & 0 & 0 & 0 & 0 & 0 \\ M_u & 0 & 0 & 0 & M_q & 0 & 0 & 0 & 0 \\ 0 & 0 & 0 & 0 & 0 & N_r & 0 & 0 & 0 \\ 0 & 0 & 0 & 1 & 0 & 0 & 0 & 0 & 0 \\ 0 & 0 & 0 & 0 & 1 & 0 & 0 & 0 & 0 \\ 0 & 0 & 0 & 0 & 0 & 1 & 0 & 0 & 0 \end{bmatrix} \tag{5}$$

$$\mathbf{B} = \begin{bmatrix} X_{\delta_x} & 0 & 0 & 0 \\ 0 & Y_{\delta_y} & 0 & 0 \\ 0 & 0 & 0 & Z_{\delta_0} \\ 0 & L_{\delta_y} & 0 & 0 \\ M_{\delta_x} & 0 & 0 & 0 \\ 0 & 0 & N_{\delta_p} & 0 \\ 0 & 0 & 0 & 0 \\ 0 & 0 & 0 & 0 \\ 0 & 0 & 0 & 0 \end{bmatrix} \tag{6}$$

where g is the only non-derivative parameter, representing the gravitational constant as $9.806\,\mathrm{m/s^2}$. Calculating the eigenvalues of the system without any control input ($\mathbf{u} = \mathbf{0}$) yields the poles of the system, which reveal information about the dynamic modes. The poles of the linear quadrotor models at hover for all four canting variants are shown in Figure **10**, while Figure **11** focuses on these poles in three regions revealing their dependence on differential torsional canting. In total, there are four stable poles located on the real axis for each model variant. These modes represent the critically damped ($\zeta = 1$) subsidences following a pitch, roll, yaw or heave perturbation.

As the cant angle increases, the pitch and roll subsidences decrease in frequency, and therefore move towards the origin on the real axis as shown in Figure **11a**. Furthermore, the separation between the frequencies of the roll and pitch subsidences increases, as the roll subsidence moves further towards the origin than the pitch subsidence. This asymmetric separation behaviour occurs due to the pitch-up moment (M_{χ_d}) resulting from the combination of the vertical rotor separation and differential torsional cant, as depicted in Figure **9** and discussed in Section **3**. On one hand, a positive canting modification ($\chi_d > 0$) reduces M_u, as the front rotors experience favourable free-stream components with forward flight speed, whereas the rear rotors are exposed to less favourable free-stream components due to backward tilt about the y-axis (see θ_i in Figure **4**). On the other hand, this reduction is mitigated by counteracting M_{χ_d}.

The yaw subsidence shows a notable pole movement with respect to increasing cant angle, as shown in Figure **11b**. Initially, the pole moves towards the unstable region for $\chi_d = 2.5°$. This is followed by a direction change for $\chi_d = 5°$ and $\chi_d = 7.5°$, where the pole starts to move away from the unstable region. It appears that there is a local minimum for the yaw damping derivative out of all the investigated cases at $\chi_d = 2.5°$ (see Table **3**), which is broadly discussed in following dedicated subsection.

The open-loop dynamics exhibit oscillatory unstable modes for perturbations in roll and pitch, which are referred to as phugoid motion (Figure **11c**). With increasing χ_d, the unstable roll phugoid increases in frequency, whereas the unstable pitch phugoid decreases. This means that canting results in a quicker roll and a slightly slower pitch phugoid motion, confirming Niemiec et. al. [5] regarding the changes in the roll and pitch responses that was mentioned in Section **1**. It is also worthy to note that the roll phugoid poles move along an almost constant negative damping ratio ($\zeta < 0$), whereas the pitch phugoid poles tend to decrease in ζ with increasing χ_d, by moving little less away from the baseline pole towards the origin. Similar to the pitch roll subsidences, this asymmetric behaviour in the pitch phugoid pole movement occurs due to emerging M_{χ_d} from vertical rotor separation.

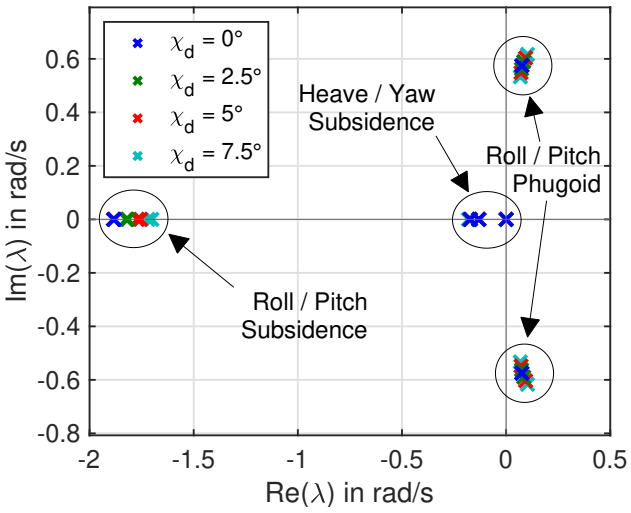

Figure 10 Pole locations at hover state

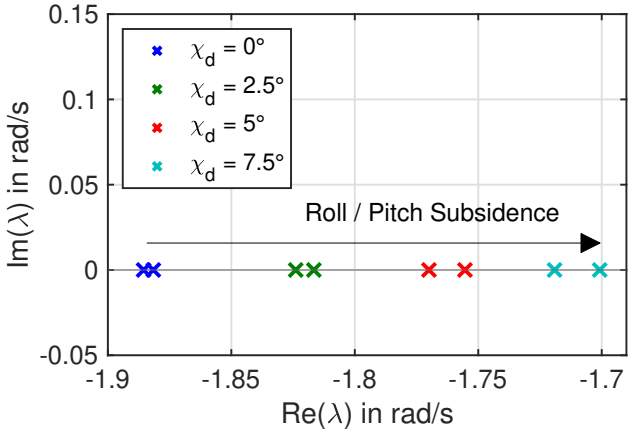

(a) Pitch and roll subsidence

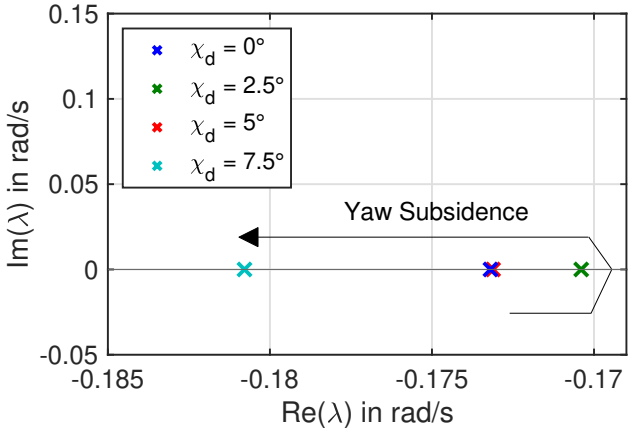

(b) Yaw subsidence

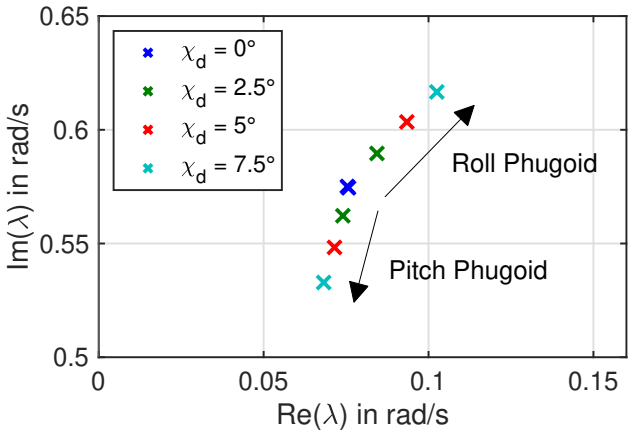

(c) Pitch and roll phugoid (upper half)

Figure 11 Pole behaviours due to χ_d at hover state

Yaw Deficiencies

Previous piloted simulator campaign results [2] showed discrepancies between the predicted handling qualities from linear model analysis and the assigned handling qualities ratings. Due to the yaw moment generation of a multirotor by varying rotor rpm, the overall achievable yaw bandwidth is low compared to vehicles with a dedicated tail rotor. However, a predicted Level 3 yaw bandwidth axis was not found to influence the assigned ratings as expected [2]. The lowest awarded ratings were at Level 2 for all tested MTEs, which were expected to be affected the most by the bandwidth criteria, namely the precision tasks Hover, Hover Turn and Pirouette [2]. This indicates that the influence of poor predicted levels in yaw axis likely will not correlate with the assigned levels for multirotor configurations as it does for helicopters. The assumption is that this is mainly due to the weak coupling between the heave and yaw axes.

For heave/yaw-coupled aircraft in a precision height hold task, the pilot has to compensate each and every small collective input with a corresponding pedal input in order to counteract the coupled yaw response. Therefore, the yaw bandwidth is closely related the to assigned ratings of such systems.

For heave/yaw-uncoupled aircraft, the yaw bandwidth would only be tested in closed-loop precision heading tracking requirements, which could be argued as not part of the commonly tested low-speed MTEs, with the possible exception of the Hover Turn MTE. The second anomaly was specifically the assigned ratings for the Hover Turn, which was also located in the Level 2 region. Here, the bandwidth was expected to have an even higher impact on the rating due to the precise heading capture requirement of the task. However, the pilots stated that the main aspect that effected the awarded ratings was the sluggish response of the yaw axis, requiring aggressive pedal inputs and compensation afterwards. This upshot indicates that an improvement in the moderate to large amplitude - low to moderate frequency attitude changes (attitude quickness) might have a bigger impact on the handling qualities, rather than the small amplitude/moderate to high frequency response as previously assumed (bandwidth/phase delay).

When looking at the linear state-space representation of the quadrotor model, given by Eq. (3) and (5), the two derivatives influencing the overall yaw performance are the yaw damping (N_r) and the pedal control sensitivity (N_{δ_p}). The numerical values for the increase in the cant angle are given by Table **3**. For helicopters in hover, N_r is almost entirely due to the tail rotor, with a numerical value between -0.25 and -0.4, depending on the tail rotor design parameters [15]. The baseline quadrotor model shows a significantly lower yaw damping derivative compared to those of conventional helicopters. As χ_d increases, so does N_r in negative sense. However, even at high canting angles, such as $\chi_d =$

$7.5°$, N_r does not reach -0.25. Therefore, substantial increase in yaw damping will be needed in the form of response quickening control augmentation, and cannot be achieved by the canting of the rotor alone. Based on this conclusion, the piloted simulations were conducted with the involvement of an ACAH flight control system, which is described in Section **5.2**.

Table 3 Influence of χ_d on the yaw damping derivative and pedal control sensitivity derivative

χ_d [°]	N_r [1/s]	N_{δ_p} [rad/s^2%]
0	-0.173	0.009
2.5	-0.170	0.016
5	-0.173	0.030
7.5	-0.181	0.031

The pedal control derivative (N_{δ_p}) is defined as the initial angular acceleration per unit of control input (in this case percent of total stick displacement), and is recognized as a primary parameter affecting pilot opinion of aircraft handling [15]. Here, significant improvements for increase in cant angle can be seen. For $\chi_d = 7.5°$, the control sensitivity is increased by $244\,\%$ accompanied by a maximum of $5\,\%$ increase in the total power. An increase of $77\,\%$ in the control sensitivity can be obtained with $\chi_d = 2.5°$.

Overall, an increase in cant angle results in higher control sensitivity in the yaw axis. The $\chi_d = 2.5°$ variant is of special interest: The yaw damping remains the lowest while still assuring increase in control sensitivity by a factor of 1.77. In addition, the decrease in roll phugoid stability is the smallest of the evaluated cant angle variants. The reduction of the yaw damping results in a lower bare airframe yaw bandwidth. Nevertheless, the initial results showed that bandwidth has little impact on assigned ratings due to the fact that small amplitude high frequency pedal corrections due to collective inputs are rarely needed in the quadrotor configuration during low-speed MTEs. With the goal in mind to increase moderate to large amplitude or low to moderate frequency attitude response, the $\chi_d = 2.5°$ configuration was selected for the piloted handling qualities evaluations.

5. HANDLING QUALITIES ASSESSMENTS

The baseline variant ($\chi_d = 0°$) and a modified quadrotor variant ($\chi_d = 2.5°$) were assessed regarding their handling qualities using the two methods stated in ADS-33E [3]: predicted and assigned levels. The former is a criteria-based objective assessment method examining the flying qualities parameters obtained from the vehicle response to different input types (step input, frequency-sweep, etc.). The latter is a subjective assessment method awarded by the test pilots with respect to the Cooper-Harper Handling Qualities Rating Scale (HQR, see Figure **A.1**) [4] upon performing certain flight tasks called Mission Task Elements (MTEs). Here, the main focus of HQR is to determine the workload regarding performed pilot control compensation to complete the MTE. Eventually, both methods return a level index outlining the adequacy of the model for each obtained flying qualities parameter, as well as for each assigned HQR: Level 1, Level 2, and Level 3, representing minimal-, moderate-, and extensive pilot workload, respectively [15].

The virtual flight test campaign took place in the flight simulator facility AVES. In contrast to the analyses in the previous two sections, both quadrotor variants were augmented with simple flight controllers for the handling qualities assessments. The predicted and assigned levels were obtained using selected criteria and MTEs from the ADS-33E [3]. In addition to HQR, the model variants were also rated on the flown MTEs using Bedford Workload Scale (BWS, see Figure **A.2**) [16, 17] , which determines the workload in terms of the potentially available spare capacity of the pilot for a secondary task, such as monitoring crew members, looking outside, listening and responding to the radio calls. The results were compared with the conventional helicopter configuration, ACT/FHS [8], which is a highly modified version of an EC135.

Following sections elaborate on the selected criteria and MTEs, the setup of the simulation and the conduction of the flight tests for both methods. Finally, the assessment results are given.

5.1. Selected Criteria and MTEs

Unlike in the previous study [2], the main focus of the criteria and MTE selections lies on assessing the effect of the canting modification on the response of the vehicle to inputs with different dynamic amplitudes and frequencies about the three axis. Three types of dynamic inputs have been targeted as classified in ADS-33E [3]:

- Small amplitude - moderate to high frequency,
- Small amplitude - low to moderate frequency,
- Moderate amplitude - low to moderate frequency.

In that regard, six ADS-33E criteria have been selected for the assessment of the predicted levels about the three axes:

- **Bandwidth** in *Pitch*, *Roll* and *Yaw Axes*,
- **Dynamic Stability** in *Pitch* and *Roll Axes*,
- **Attitude Quickness** in *Yaw Axis*.

Based on the expected impact of canting modification on the pilot rating and anticipated relevancy for quadrotor configurations in low-speed regime, following ADS-33E MTEs have been selected for the piloted study:

- **Hover** to test the impact of canting modification on the dynamic stability in roll and pitch,
- **Hover Turn** to identify the changes in yaw sensitivity due to rotor canting during the heading change section.
- **Pirouette** to test the impact of canting modification on the ability to accomplish precision control of the vehicle simultaneously in all axes.

For all selected MTEs, the performance limitations refer to the Cargo/Utility Aircraft category with conditions for GVE (clear daylight & adequate visual cues) and no-wind.

5.2. Simulaton Setup

AVES features a replica of the ACT/FHS helicopter cockpit with conventional helicopter flight controls. The helicopter cockpit was considered adequate for the simulation campaign, although it does not directly represent the cockpit of quadrotor eVTOLs. To represent the studied configuration in the flight tests, an eVTOL external visual model with a high-aft rotor arrangement was chosen (Figure **12a**). With the forward rotors being visible within the cockpit sight (Figure **12b**), it was intended to give the pilots a higher perception of flying in a quadrotor rather than sitting in a standard helicopter. A flight test scenario consists of a generic MTE test course including visual cues (hover boards, ground markings, etc.), designed in compliance with the ADS-33E MTEs for Utility/Cargo Aircraft category and GVE. The quadrotor flight models were run in HOST, whereas the flight model of the ACT/FHS was run in DLR's in-house flight dynamics code.

The stability augmentation features an ACAH response type in pitch and roll. In terms of directional and heave control, a simple rate damping feedback in yaw and a RC response type in heave were respectively used. Although this work is not focused on flight control system augmentation, it was deemed necessary to include a control augmentation system, especially in the lateral and longitudinal axis, based on prior results [2]. The tuning of the control system is based on Level 1/Level 2 optimization for the ACT/FHS helicopter model. The control tuning was then evaluated using the baseline quadrotor model without canting and was found to yield boundary Level 1/Level 2 conditions. Thus, it was refrained from returning the control parameters. Although a dedicated tuning for each canting variant would be desirable to improve the overall handling qualities even further, such modification would potentially also wash-out any direct impact of canting on the ratings assigned by the pilots.

5.3. Conduction of the Simulator Tests

For the assessment of the predicted levels, sweep, step and pulse responses of the augmented nonlinear real-time quadrotor and ACT/FHS models at hover were recorded. The results were evaluated with respect to the aforementioned selected criteria.

(a) Outside view

(b) Cockpit view

Figure 12 Virtual quadrotor model in AVES

The virtual flight test campaign was conducted with a single helicopter experimental test pilot, highly experienced in light utility helicopters*. Due to the unusual flight characteristics of the quadrotor, a relatively long familiarization time was needed for the pilot to adopt his control strategy and to minimize training effects. After familiarization with each new test case, the pilot was asked to perform 2-4 repetitions and give a representative rating for the final run. In particular for the HQR, a task performance display specified for each MTE was shown to the pilot after each run to support the subjective rating with objective performance data, such as ground track, attitude, altitude and time.

5.4. Results

The results for the predicted and assigned levels are shown in Figure **13** and Figure **14** respectively. The former depicts the level classification of the baseline quadrotor ($\chi_d = 0°$), modified quadrotor ($\chi_d = 2.5°$) and the ACT/FHS based on the results obtained from the previously mentioned criteria, while the latter shows the results of the subjective pilot ratings for each MTE with respect to HQR. The assigned workload ratings with respect to BWS are shown in Figure **15**.

Predicted Levels

The bandwidths for pitch and roll are located in the Level 1 region for all examined configurations (see Figures **13a** and **13b**). Except for the roll bandwidth, the canted model exhibits higher bandwidth values compared to the uncanted baseline model. Increasing the cant angle to $\chi_d = 2.5°$ moves the dynamic roll stability (Figure **13e**) metric along the Level 1 / Level 2 border region, effectively moving the poles upwards along the constant damping ratio line $\zeta = 0.35$, whilst increasing in natural frequency ω_n. This is congruent with the observations made in the linear analysis, where the roll phugoid mode exhibits a similar trend for increase in cant angle, albeit in the unstable region due to a lack of stabilizing flight control feedback. The same holds for the dynamic pitch stability (Figure **13d**). Based on the linear model analysis, the expectation would have been a decrease in natural frequency whilst moving along the $\zeta = 0.35$ line. This behavior could be explained by the introduction of the FCS feedback providing the ACAH response type, but needs further investigation to be conclusive.

*Over 6850 flight hours, 42 years under license, type ratings for EC-135, Bo-105, CH-53 and UH-1D

The bandwidths for the yaw axis (Figure **13c**) are located in the Level 1 region for all examined configurations. The modified variant shows higher bandwidth values compared to the baseline variant. Yaw quickness (Figure **13f**) is improved from Level 2 to Level 1 with the introduction of the rotor cant angle. This again is reflected by a significant increase in pedal control sensitivity observed in the linear analysis. Compared to the quickness value of a helicopter setup (ACT/FHS), one can see that the ACT/FHS model still shows quicker response relative to the modified quadrotor model. Overall, the most significant change in predictive handling qualities criteria between the baseline model and $\chi_d = 2.5°$ is the increase in yaw attitude quickness.

Assigned Levels

As depicted in Figure **14**, for the Hover MTE, the baseline quadrotor was awarded HQR-5. The pilot stated that the amount of aggressiveness during the transition from diagonal approach to hover stabilization had to be reduced compared to the ACT/FHS to avoid roll oscillations. Consequently, the initial control inputs to decelerate were decisive because the ability to apply corrections during the transition was limited. As a result, only adequate task performance was achieved. For the modified quadrotor, the rating improves to HQR-4, since the controllability is improved according to the pilot. The task performance improved to desired levels, although the pilot still noticed deficiencies about the roll axis. For the ACT/FHS, a rating of HQR-3 was awarded because the pilot was able to apply the aggressiveness needed to achieve the desired task performance and no oscillations occurred. The BWS-ratings given in Figure **15** are BWS-5 for both quadrotor variants and BWS-4 for the ACT/FHS because the pilot had to compensate the deficiencies in the flying characteristics of the quadrotors. In general, the workload for this MTE is driven by the transition phase, in which only a reduced available spare capacity for a secondary task was available. The pilot stated that the workload for the hover phase was much lower.

For the Hover Turn MTE, the baseline quadrotor received a rating of HQR-5 and the modified quadrotor received a rating of HQR-3. The task performance was mainly driven by holding the position by small corrections during the yaw phase. The transition to hover at the end of this MTE was less demanding, simply because there is no strict time limit for this phase. Therefore, less aggressive control inputs are sufficient, which reduce the risk of experiencing oscillations. The pilot stated that the controllability of the canted quadrotor is improved, which

results in a better HQR. The ACT/FHS received a rating of HQR-3 as well because pilot compensation was still a factor to achieve the desired task performance. However, according to the pilot, there was still a potential to fly this task more aggressively due to the better yaw characteristics. The BWS-ratings are BWS-4 for all cases because neither the yaw phase nor the transition to hover phase caused a major reduction in the available spare capacity.

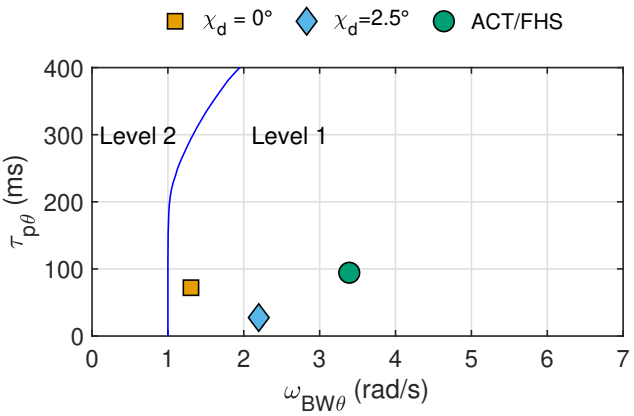

(a) Bandwidth / phase delay - pitch axis
(All other MTEs - UCE=1 and fully attended operations)

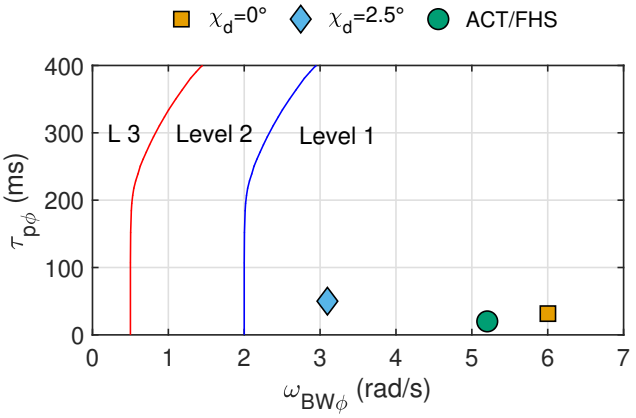

(b) Bandwidth / phase delay - roll axis
(All other MTEs - VMC, UCE=1 and fully attended operations)

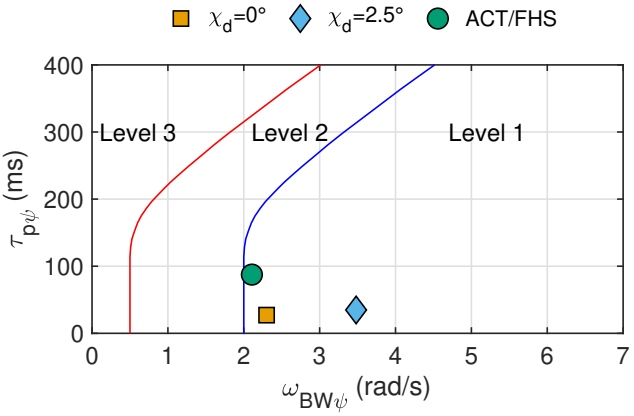

(c) Bandwidth / phase delay - yaw axis
(All other MTEs - hover and low-speed)

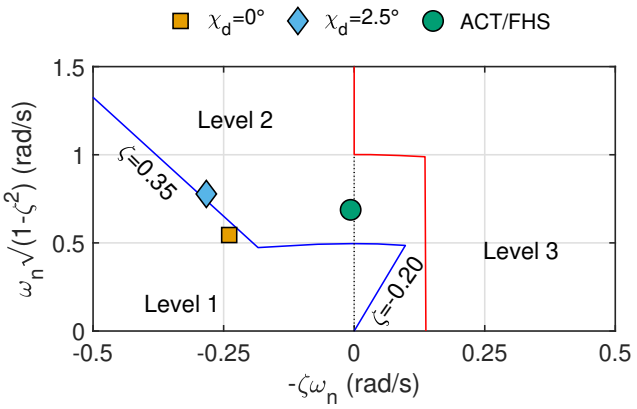

(d) Dynamic stability - pitch axis
(Fully attended operations in Hover)

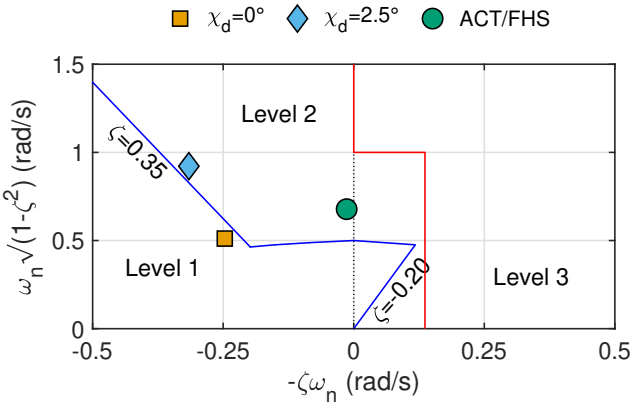

(e) Dynamic stability - roll axis
(Fully attended operations in Hover)

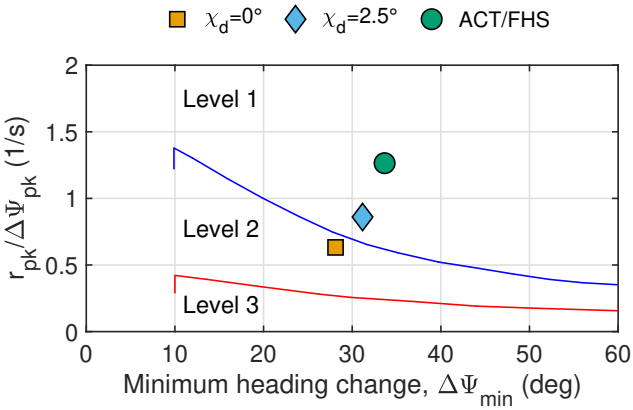

(f) Attitude quickness criterion - yaw axis
(All other MTEs)

Figure 13 Predicted handling qualities levels *(refer to ADS-33E [3] for the used symbols, acronyms and descriptions given in parentheses)*

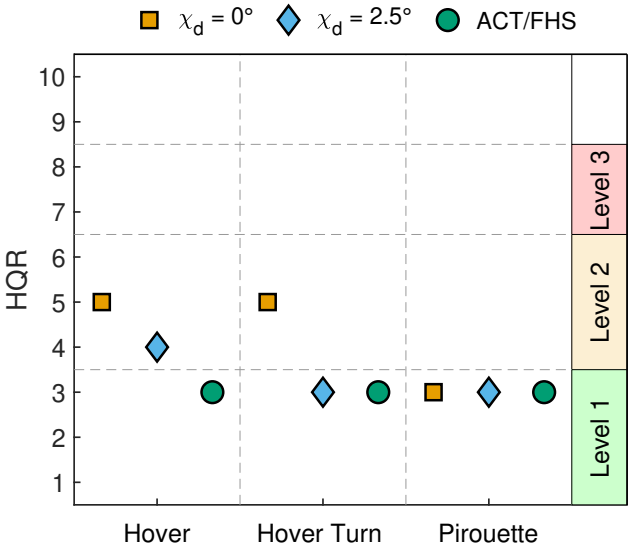

Figure 14 Assigned HQR-ratings

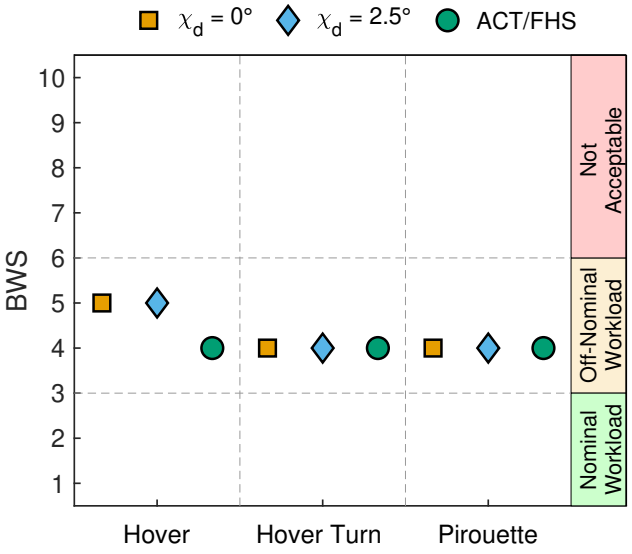

Figure 15 Assigned BWS-ratings

As all variants received a HQR-3 rating for the Pirouette MTE, the pilot stated that the ACT/FHS was the variant required the least amount of control compensations by minimal differences among all, followed by the modified quadrotor variant. It is worth to mention that the pilot was not limited by roll oscillations during the transition to hover phase, completing this phase within the required time limits. This can be associated with different demands on control inputs (mainly on roll axis instead of a combination of pitch and roll axes) and training effects during the simulation campaign. The BWS-ratings are BWS-4 for all cases, as no major reduction in the available spare capacity was perceived between the variants.

6. CONCLUSIONS

The impacts of the differential torsional canting on the flight characteristics of a passenger-grade quadrotor configuration were investigated. Model variants with different cant angles were analyzed regarding trim performance, linear flight dynamics and handling qualities. The trim analyses for hover and level flight and linear bare-airframe flight dynamics at hover state were compared between the baseline variant ($\chi_d = 0°$) and three modified variants ($\chi_d = 2.5°$, 5° and 7.5°). Finally, handling qualities assessments for the baseline variant and the $\chi_d = 2.5°$ variant were made in the flight simulator using selected criteria and MTEs from ADS-33E. Based on the results and discussions, following conclusions are noted:

- modifying the quadrotor model by differential torsional canting slightly increases the total power required,
- combining differential torsional canting with vertical rotor separation (rear rotors higher than front rotors) leads to additional pitch-up moment, requiring the rear rotors to produce higher thrust than the front rotors to maintain the moment equilibrium,
- differential torsional canting makes the roll phugoid motion faster and the pitch phugoid motions slower, where the stabilizing effect of this modification is mitigated due to vertical rotor separation,
- differential torsional canting improves the control sensitivity in the yaw axis, which was previously found as an inherent deficit of the passenger-grade quadrotor configurations,
- the assigned levels and comments of the test pilot confirmed the observable reduction of the required control compensation due to differential torsional canting during performing the MTEs.

Future works will mainly focus on two aspects in terms improving the modeling capabilities for simulation-mature eVTOL configurations based on the knowledge gained during this study. The first aspect is the development of the design and sizing rules for eVTOL multirotor configurations. The second aspect is the task-tailored design of an automatic control system and investigation of the interactions between control tuning parameters, rotorcraft design parameters and handling qualities requirements for eVTOL configurations.

REFERENCES

[1] The Vertical Flight Society, "eVTOL aircraft directory." `https://evtol.news/aircraft`, 2022. [accessed 28-April-2022].

[2] K. Atci, M. Jones, and T. Jusko, "Assessment of the handling qualities of multirotor configurations using real time simulation," in *Deutscher Luft- und Raumfahrtkongress 2021*, (Virtual & Bremen, Germany), Sept. 2021.

[3] Anonymous, "Aeronautical design standard performance specification handling qualities requirements for military rotorcraft," Technical Report ADS-33E-PRF, United States Army Aviation and Missile Command Aviation Engineering Directorate, Redstone Arsenal, Alabama, Mar. 2000.

[4] G. E. Cooper and R. Harper, "The use of pilot ratings in evaluation of aircraft handling qualities," NASA Technical Note TN D-5153, NASA, Ames Research Center Moffett Field, CA, USA, 1969.

[5] R. J. Niemiec and F. Gandhi, "Effect of rotor cant on trim and autonomous flight dynamics of a quadcopter," in *AHS International 74th Annual Forum and Technology Display*, (Phoenix, AZ), May 2018.

[6] C. M. Liersch and M. Hepperle, "A distributed toolbox for multidisciplinary preliminary aircraft design," *CEAS Aeronautical Journal*, vol. 2, pp. 57–68, Aug. 2011.

[7] B. Benoit, A.-M. Dequin, K. Kampa, W. von Grünhagen, P.-M. Basset, and B. Gimonet, "HOST, a general helicopter simulation tool for Germany and France," in *AHS, 56th Annual Forum and Technology Display*, (Virginia Beach, VA), May 2000.

[8] H. Duda, S. K. Advani, and M. Potter, "Design of the DLR AVES research flight simulator," in *AIAA Modeling and Simulation Technologies (MST) Conference*, (Boston, MA), p. 4737, Aug. 2013.

[9] M. Siggel, J. Kleinert, T. Stollenwerk, and R. Maierl, "TiGL: An open source computational geometry library for parametric aircraft design," *Mathematics in Computer Science*, vol. 13, pp. 367–389, July 2019.

[10] C. Malpica and S. Withrow-Maser, "Handling qualities analysis of blade pitch and rotor speed controlled eVTOL quadrotor concepts for urban air mobility," in *VFS International Powered Lift Conference 2020*, (San Jose, CA), Jan. 2020.

[11] W. Johnson, C. Silva, and E. Solis, "Concept vehicles for VTOL air taxi operations," in *AHS Conference on Aeromechanics Design for Transformative Vertical Flight*, (San Fransisco, CA), Jan. 2018.

[12] W. Johnson and C. Silva, "Observations from exploration of VTOL urban air mobility designs," in *7th Asian/Australian Rotorcraft Forum*, (Jeju Island, Korea), Nov. 2018.

[13] M. D. Patterson, K. R. Antcliff, and L. W. Kohlman, "A proposed approach to studying urban air mobility missions including an initial exploration of mission requirements," in *AHS International 74th Annual Forum & Technology Display*, (Phoenix, AZ), May 2018.

[14] C. Silva, W. R. Johnson, E. Solis, M. D. Patterson, and K. R. Antcliff, "VTOL urban air mobility concept vehicles for technology development," in *2018 Aviation Technology, Integration, and Operations Conference*, American Institute of Aeronautics and Astronautics, June 2018.

[15] G. D. Padfield, *Helicopter flight dynamics: the theory and application of flying qualities and simulation modelling*. Oxford Washington DC: Blackwell Pub. American Institute of Aeronautics and Astronautics, 2007.

[16] A. H. Roscoe and G. A. Ellis, "A Subjective Rating Scale for Assessing Pilot Workload in Flight: A decade of Practical Use," Technical Report TR 90019, Royal Aircraft Establishment, Farnborough, UK, Mar. 1990.

[17] Anonymous, "NASA Space Flight Human System Standard Volume 2: Human Factors, Habitability, and Environmental Health," Technical Report NASA-STD-3001, Volume 2, Revision C, National Aeronautics and Space Administration (NASA), Washington D.C., USA, Apr. 2022.

A. RATING SCALES

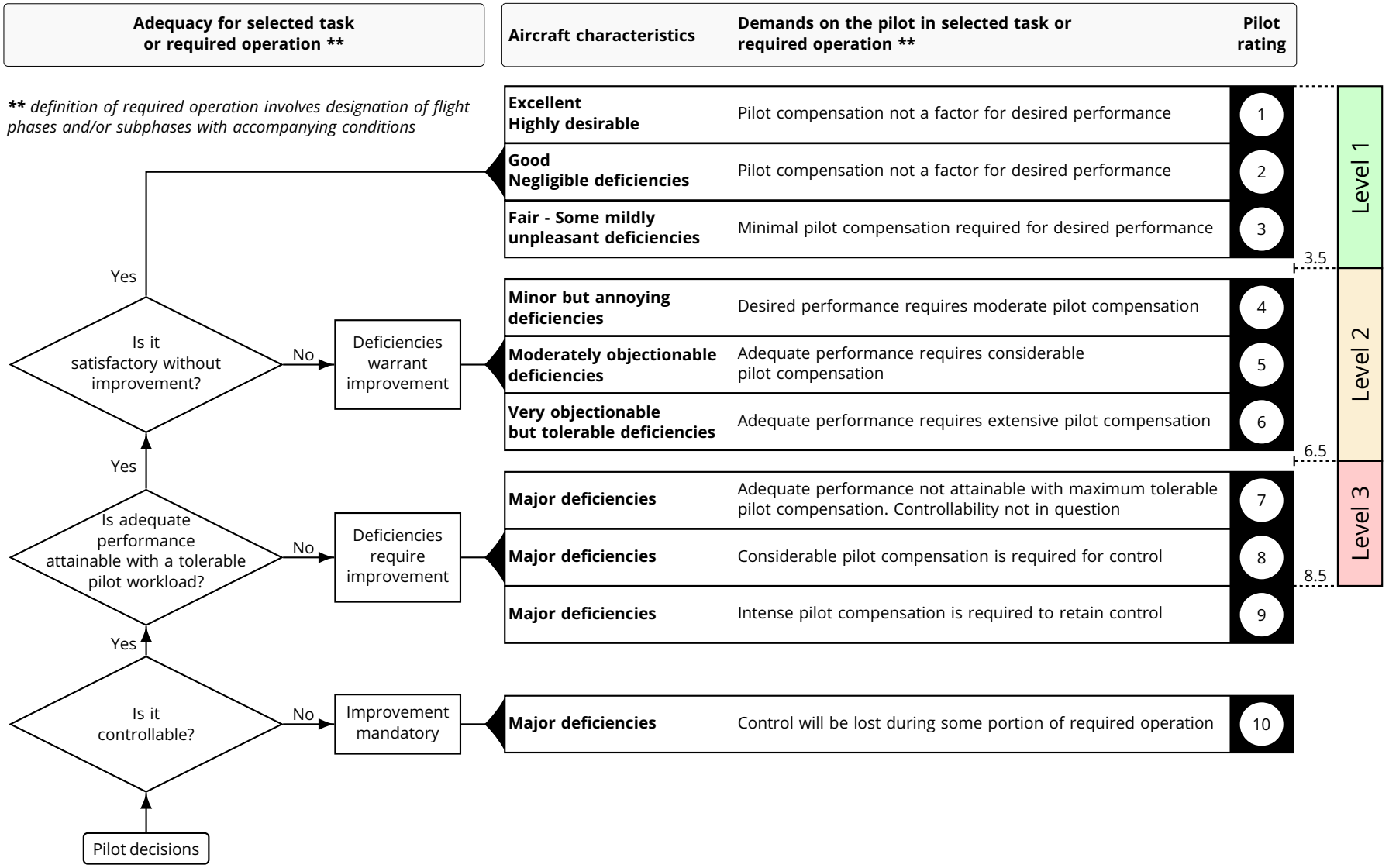

Figure A.1 Cooper-Harper Handling Qualities Rating Scale (HQR) [4] - level categorization according to ADS-33E [3]

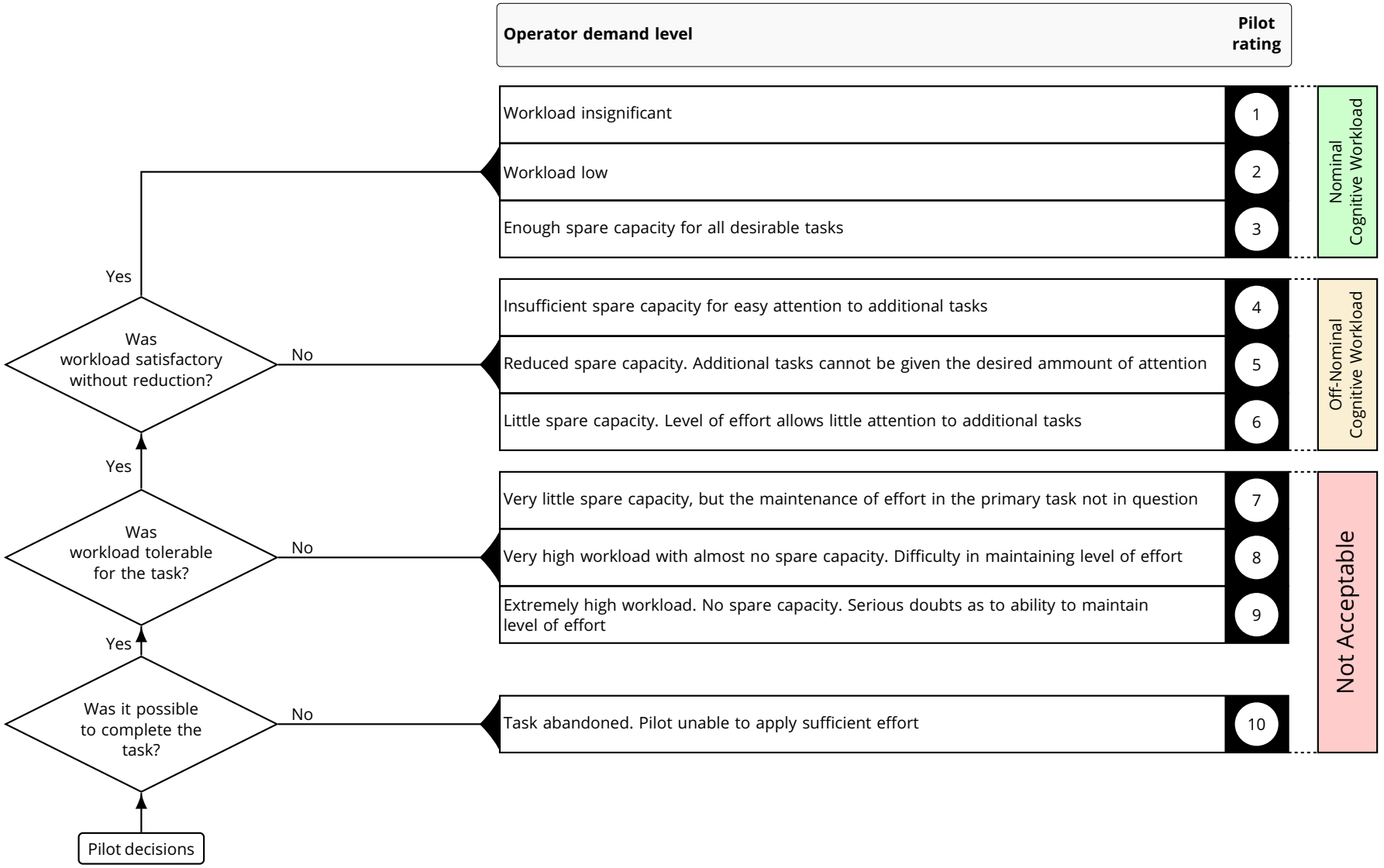

Figure A.2 Bedford Workload Scale (BWS) [16] - workload categorization according to NASA-STD-3001 [17]